Atmos. Meas. Tech. Discuss., 7, 6877–6915, 2014
www.atmos-meas-tech-discuss.net/7/6877/2014/
doi:10.5194/amtd-7-6877-2014

Atmospheric Measurement Techniques Discussions

Development and validation of inexpensive, automated, dynamic flux chambers

B. B. Almand-Hunter[1], J. T. Walker[2], N. P. Masson[1], L. Hafford[1], and M. P. Hannigan[1]

[1]Mechanical Engineering Department, University of Colorado, 427 UCB, Boulder, CO, 80303, USA
[2]Air Pollution Prevention and Control Division, National Risk Management Research Laboratory, US Environmental Protection Agency, E305-2, MD-63, Research Triangle Park, NC 27711, USA

Received: 15 May 2014 – Accepted: 19 June 2014 – Published: 10 July 2014

Correspondence to: B. B. Almand-Hunter (berkeley.almand@colorado.edu)

Published by Copernicus Publications on behalf of the European Geosciences Union.

Abstract

We developed and validated an automated, inexpensive, and continuous multiple-species gas-flux monitoring system that can provide data for a variety of relevant atmospheric pollutants, including O_3, CO_2, and NO_x. Validation consisted of conducting concurrent gas-phase dry-deposition experiments, using both dynamic flux chambers and an eddy-covariance system, in a grassy clearing in the Duke Forest (Chapel Hill, NC). Experiments were carried out in June and September, under a variety of meteorological conditions. Ozone-deposition measurements from the two methods matched very well (4–10 % difference in mean flux rate) when the leaf-area index (LAI) inside the chambers was representative of the average LAI in the field. The dynamic flux chambers can be considered an accurate measurement system under these conditions. CO_2 measurements were conducted for one 20 h period, and the flux chamber captured the diurnal trend in CO_2 flux well, although the quantity of the data was not sufficient to validate chamber performance. Flux-chamber NO_x measurements could be calculated when ambient NO_x concentrations were above 1 ppb. Unfortunately, the eddy-covariance system for measuring NO_x was not available during this field campaign, so comparisons cannot be made. NO_x fluxes were in a reasonable range for the field site.

1 Introduction

Deposition of pollutants, including ozone, nitrogen, and acidic compounds (SO_x, NO_y), places environmental stress on sensitive vegetated landscapes and aquatic ecosystems (EPA, 2011; Williams and Tonnessen, 2000; Fangmeier et al., 1994). Examples of this stress include increased susceptibility to illness and decreased growth for sensitive plant species (EPA, 2011, 2006), decreased water quality, toxicity to freshwater organisms, eutrophication, change in greenhouse emissions from soil (Fenn et al., 1998), reduction in biodiversity, and interference with a plant's uptake of other important cations,

AMTD
7, 6877–6915, 2014

such as potassium (Fangmeier et al., 1994). These negative effects can be particularly pronounced at high altitudes, where buffering capacities can be below average (Fenn et al., 1998; Williams and Tonnessen, 2000; Benedict et al., 2013).

Dry deposition, which is the process by which pollutants are transported from the atmosphere to the earth's surface without precipitation (Seinfeld and Pandis, 2006), is an important component of atmospheric deposition. This process is estimated to account for up to 50 % of total atmospheric deposition in the United States (EPA, 2010; Wesely and Hicks, 2000). Despite this sizable contribution to total atmospheric deposition, there is a lack of direct measurements for sulfur and nitrogen dry-deposition in the US. Currently employed direct dry-deposition measurements are not part of the routine measurement suite (Clean Air Status and Trends Network) because they are prohibitively expensive and complex. This results in significant uncertainty in deposition loads, specifically regarding transfer ratios (the relationship between ambient concentrations and total deposition). Given the large spatio-temporal variability in air-surface exchange rates of reactive compounds, there is a need for low-cost, easily deployable systems to measure dry deposition directly. These measurement devices should be automated and remotely controlled, so that they can be deployed for extended periods of time without excessive maintenance.

There has been significant debate over whether ozone damage to vegetation is best quantified and regulated using ambient concentrations or atmospheric fluxes (EPA, 2006; Musselman et al., 2006). While the use of ambient concentrations is certainly much simpler, fluxes have more physical meaning. Understanding deposition and emission rates is an important piece of estimating atmospheric concentrations in the planetary boundary layer for climate and weather models. Since it is not possible to measure flux everywhere, improving deposition models is a crucial step in determining accurate transfer ratios. Efforts to improve models are ongoing (Zhang et al., 2001, 2003; Brook et al., 1999; Schwede and Lear, 2014); models estimate flux well under some conditions, but fluxes determined by different models and observations can vary by a factor of 2 to 3 (Schwede et al., 2011; Wu et al., 2011; Flechard et al., 2011). Direct

AMTD
7, 6877–6915, 2014

dry-deposition measurements are needed to improve and validate models for different ecosystems, and under varied environmental conditions.

Currently, the most accurate direct method for measuring atmospheric fluxes is eddy covariance (Seinfeld and Pandis, 2006; Turnipseed et al., 2009). Eddy covariance consists of taking high-speed measurements of concentration and three-dimensional wind velocity. The flux is computed from the covariance between the fluctuating components of wind velocity and concentration (Turnipseed et al., 2009). This method is the most mathematically robust and accurate way to acquire dry-deposition measurements, but it is expensive and technically difficult compared with indirect measurement methods (Baldocchi et al., 1988).

Another method for measuring flux, which is used more frequently to measure emissions than it is to measure deposition, is the flux chamber. Advantages of flux chambers over eddy covariance include reduced cost, the ability to determine spatial variability in deposition, the ability to take measurements in areas with complex topography and areas with non-uniform vegetation (eddy-covariance typically requires an area of uniform vegetation that is $\geq 100\,m^2$), mobility, and the potential to be used with inexpensive sensors (Horst and Weil, 1994). The main drawback of using chambers for flux measurements is that they alter the environment in which they are placed. Static chambers, which are commonly used to measure emissions, significantly affect environmental conditions (Pape et al., 2009).

Dynamic flux chambers minimize the alteration of environmental conditions by constantly pumping ambient air into the chamber. Table 1 lists previous flux-chamber measurements of NO, NO_2, CO_2, and O_3. One type of flux chamber listed in Table 1 is the leaf-scale dynamic chamber, which is used to measure fluxes to and from individual leaves and branches (Breuninger et al., 2013, 2012; Geßler et al., 2000; Sparks et al., 2001; Altimir et al., 2002). While leaf-scale deposition measurements are important for understanding plant dynamics, they can be difficult to translate to the canopy scale, and do not directly represent ecosystem-level flux.

AMTD
7, 6877–6915, 2014

Another type of chamber listed in Table 1 is the dynamic soil-flux chamber (Remde et al., 1993; Butterbach-Bahl et al., 1997; Norman et al., 1997). A significant portion of the chambers listed did not have open tops, and the soil or vegetation in the chamber was only exposed to ambient conditions via air pumped into the chamber. These chambers, which are not normally open to the ambient environment, have significant drawbacks. They all block a fraction of incoming solar radiation, and in order to maintain ambient conditions, they have to be moved frequently, which makes long-term or remote deployments difficult.

Several research groups have addressed these issues by developing chambers with lids that open and close automatically (Meixner et al., 1997; Pape et al., 2009; Kitzler et al., 2006). These automatic chambers operate in a normally open mode, with lids that close for just a few minutes per hour. Provided that the chambers are made out of highly transparent materials, so sunlight can reach the vegetation inside, the environmental conditions in the chamber remain very close to ambient (Pape et al., 2009).

While many chamber measurements have been made (Table 1), very few of these studies compare NO, O_3, and CO_2 fluxes measured by chambers to measurements acquired via micrometeorological techniques. Several groups have compared chamber measurements NO fluxes from soils to gradient measurements (Parrish et al., 1987; Kaplan et al., 1988; Stella et al., 2012). Norman and coworkers (1997) compared several types of static and dynamic chambers with each other and eddy correlation for measuring CO_2 fluxes in forest soils, but only two data points for eddy correlation were available for comparison, each representing one day. Li and coworkers (1999) compared chamber measurements of NO fluxes from agricultural soils with eddy-correlation measurements, and found that the fluxes measured by the chambers were higher than the eddy-correlation measurements, but followed a similar diurnal trend. Pape and coworkers (2008) compared an automatic, dynamic flux chamber with an eddy-covariance system at a grassland site, and demonstrated good agreement for CO_2 deposition. Due to the fact that these comparison studies are limited in number,

AMTD
7, 6877–6915, 2014

and sometimes did not yield good agreement between methods, further comparisons of flux chambers and micrometeorological methods are warranted.

Our research effort expands on this validation-based flux-chamber development through the creation of an automated, inexpensive, and continuous multiple-species gas-flux monitoring system, which can provide data for a variety of relevant atmospheric pollutants, including O_3, CO_2, and NO_x. The chambers have automatic lids, which keeps the environment in the chambers close to ambient, and eliminates the need to regularly remove them from sampling plots. This project is unique, because, in addition to contributing to the very limited chamber-validation literature, our chambers are designed to be very inexpensive (< USD 2000 each). The chambers are equipped with inexpensive metal-oxide O_3 and NO_2 sensors, which cost between USD 10 and USD 100, and our ultimate goal is to obtain fluxes using these inexpensive sensors. The first step toward reaching that goal is to use data from established O_3, CO_2, and NO_x monitors to validate the dynamic flux-chamber measurements, which enables us to isolate the uncertainty related to the use of inexpensive sensors from chamber performance. We present preliminary results, comparing chamber fluxes to eddy-covariance fluxes for O_3 and CO_2, and present NO_x fluxes measured by the flux chamber.

2 Methods

2.1 Overview

We conducted gas-phase dry-deposition experiments in a grassy clearing in the Blackwood Division of Duke Forest in Orange County, North Carolina, USA (35.97° N, 79.09° W). The field is 480 m × 305 m, and the vegetation is primarily tall fescue (Festuca arundinacea Shreb.), which is a common C3 grass in the southeastern United States. Less-prominent vegetation includes C3 and C4 grasses, herbs, and forbs, which are present in smaller amounts (Fluxnet, 2013).

AMTD
7, 6877–6915, 2014

We used five pairs of acrylic-glass flux chambers to measure dry deposition of NO_x, O_3, and CO_2 to the grassland vegetation. Experiments were carried out in June and September, under a variety of meteorological conditions. We compared the chamber results with eddy-covariance measurements, which were conducted by the EPA at the same site.

2.2 Eddy-covariance measurements

Briefly, the eddy covariance approach (Baldocchi et al., 1988) for measuring the vertical exchange of momentum, heat, and mass is based on the simplified form of the mass balance for a scalar (c), at time (t), in a notional control volume, at height (z) within the surface layer, expressed as:

$$\frac{\overline{\partial c}}{\partial t} + \frac{\partial \overline{wc}}{\partial z} = \overline{S}\delta(z), \tag{1}$$

where $\overline{wc}$ is the total covariance of c and the vertical velocity, w, S is the surface exchange rate, and $\delta(z)$ is the Dirac delta function. Overbars denote Reynold's averaging. If the scalar field is stationary, the first term on the left-hand side of Eq. (1) reduces to zero. After integrating from $z = 0$ to the top of the control volume (h), Eq. (1) further reduces to

$$\overline{wc}(h) = S. \tag{2}$$

Finally, the total covariance, $\overline{wc}$, is decomposed into mean ($\overline{\overline{wc}}$) and fluctuating ($\overline{w'c'}$, i.e., eddy flux) components, using an appropriate averaging operation (i.e., Reynolds decomposition), such that $\overline{wc} = \overline{\overline{wc}} + \overline{w'c'}$. Assuming that the mean vertical velocity is zero, the surface exchange (S) becomes equivalent to the eddy-covariance flux:

$$F = \overline{w'c'}, \tag{3}$$

AMTD
7, 6877–6915, 2014

where the overbar represents time averaging, usually 30 min, and the primes represent deviations from the mean, e.g.,

$$c' = c - \overline{c}. \quad (4)$$

Above-canopy fluxes of CO_2, H_2O, O_3, sensible heat, and momentum were measured using an instrument package, which consisted of an R.M. Young sonic anemometer (Model 81000V, Traverse City, MI), aspirated thermocouple (Model ASPTC, Campbell Scientific, Logan, UT), LI-COR (Lincoln, NE) Model 7500 (CO_2 and H_2O) open path infrared gas analyzer (IRGA), and a custom fast chemiluminescence O_3 sensor, positioned at 2.5 m above the canopy. Gas-phase instruments were calibrated weekly by mass flow controlled dilution of compressed gas standards with clean air. Wind speed components (u, v, w), temperature, and air concentrations were sampled at a frequency of 10 Hz, and data were recorded on a single laptop, using a custom data-acquisition system. Data were reduced to 30 min and hourly averages using a custom SAS program (SAS Institute, 2003).

Eddy-covariance O_3 fluxes were measured with a custom sensor that follows the basic design of Guesten and coworkers (1992), which consists of a pump (Model BTC IIS miniature diaphragm pump, Parker, Hollis, NH), a reaction cell, and a photomultiplier tube (Model H9306 side-on photosensor, Hamamatsu, Middlesex, NJ) (Guesten et al., 1992). While Guesten and coworkers (1992) are generally credited with developing the first of these systems for flux measurement applications, a number of variants of the original design have been developed over the following years (see Zahn et al., 2012). This measurement technique is known as "dry chemiluminescence", and the air sample passes over a disk, which is coated with Coumarin-1 dye (Bagus Consulting, Speyer, Germany). The reaction of O_3 with the dye results in luminescence, which is quantified by counting the resulting photons with a photomultiplier tube that views the reaction chamber from the side opposite the Coumarin disk. The ozone concentration is proportional to the number of photons produced. However, this is not an absolute measurement, and the disks have a limited lifetime over which the photon yield per unit

AMTD
7, 6877–6915, 2014

O_3 decreases. Thus, to calculate the absolute flux, the fast sensor must be calibrated to a second collocated sensor. The second sensor measures absolute O_3 concentrations, at a frequency consistent with the time scale of the flux, which is 30 min to one hour. The collocated instrument is a Model 205 dual-beam instrument (2B Technologies, Boulder, CO), which measures O_3 by UV absorption. Ozone fluxes were calculated from 10 Hz measurements, calibrated to the 2B sensor, using the ratio-offset method recommended by Muller and coworkers (Muller et al., 2010).

For flux calculations, 10 Hz data were subjected to spike filtering, 2-D coordinate rotation, correction for the time delay between the chemical sensor and vertical velocity, application of Webb–Pearmon–Leuning correction (CO_2, H_2O), and correction for high-frequency spectral attenuation (O_3) (Horst, 1997; Webb et al., 1980). The fast O_3 sensor has an effective time response of approximately 1.5 Hz. At lower frequencies, the cospectra of O_3 and vertical velocity match the shape of the temperature/vertical velocity cospectra well, with both following the generalized cospectral characteristics described by Kaimal and Finnigan (Kaimal and Finnigan, 1994). In this case, the method described by Horst (1997) was used to correct for spectral attenuation at frequencies > 1.5 Hz (Horst and Weil, 1994). Tests for stationarity and the presence of fully developed turbulence were also applied (Foken and Wichura, 1996).

2.3 Ancillary measurements

Ancillary measurements included net solar radiation (Rebs Q7.1 Net Radiometer, Campbell Scientific, Logan, UT), photosynthetically active radiation (Model LI190 quantum sensor, LI-COR, Inc., Lincoln, NE), soil heat flux (Model HP101 heat flux plate, Hukseflux USA, Inc., Manorville, NY), soil temperature (thermocouple, OMEGA Engineering, Stamford, CT), soil volumetric water (Model CS615 water content reflectometer, Campbell Scientific, Logan UT) leaf wetness (Model 237, Campbell Scientific, Logan UT) and rainfall (Model TE525 rain gauge, Campbell Scientific, Logan, UT). Data are recorded on a Campbell Scientific CR23X datalogger and reduced to 30 min and hourly averages.

AMTD
7, 6877–6915, 2014

2.4 Flux-chamber description

The dynamic flux chambers, which are shown in Fig. 1, were constructed using clear, cylindrically shaped acrylic. The chambers were constructed in pairs, and each pair had an open-bottomed chamber, which measured deposition to the vegetation inside, and a "blank" chamber, which had an acrylic bottom, and enabled us to measure deposition in the absence of vegetation. The "blank" measurement represents trace-gas losses to the chamber walls as well as any chemical reactions in the chamber that are unaccounted for in the flux calculations.

All of the chambers have a 45.7 cm diameter and 0.48 cm wall thickness. Four pairs of chambers have a height of 83.8 cm, and the remaining pair has a height of 58.4 cm. The chambers were designed with this height distribution because many species of natural vegetation, including grassland, are taller than 58.4 cm. The shorter chambers were designed to measure fluxes over shorter vegetation, such as alpine tundra, which is present in sensitive areas such as Rocky Mountain National Park. The shorter chambers are likely more accurate for vegetation below 59 cm tall, since they increase the ratio of vegetative surface area to volume.

The chambers were designed to minimize deposition of trace gases to the chamber walls, which was accomplished by placing the inlet and outlet holes in locations that limited contact between the flow path and the chamber walls. Ambient air enters the chambers through four holes, which are each 5.2 cm in diameter, and evenly spaced around the circumference of the chamber. The chamber outlet is at the top of the chamber, as shown in Fig. 2. The grass outside the chamber, near the inlet holes, is removed, which prevents trace gases from depositing to external vegetation before the air stream enters the chamber.

Air is pulled through the chamber by a US General 3 CFM Two-Stage Vacuum pump, and concentration samples were measured in one of two polytetrafluoroethylene (PTFE) tubes at the outlet. Gas-phase sampling is discussed in more detail in Sect. 2.5.

AMTD
7, 6877–6915, 2014

For most experiments, the pump was set to pull 80 L min^{-1} of air through the chamber. In addition to the flow induced by the vacuum pump, the 2B ozone monitor pulled approximately 1 L min^{-1}, the Thermo Scientific NO_x analyzer pulled 0.1 L min^{-1}, the LI-COR H_2O/CO_2 monitor pulled 0.25 L min^{-1}, and the small, inexpensive pump, which pulled air over the inexpensive sensors, pulled 5 L min^{-1}. Thus, the total flow rate through the chamber was 86.35 L min^{-1}, which equates to a residence time of 1.5 min. Pape and coworkers found that other researchers have operated dynamic flux chambers with residence times ranging from 10 s to 24 min, and chose to operate their dynamic flux chambers at a residence time of 40 s (Pape et al., 2009). Gillis and Miller found that changes in air-stream residence time in flux chambers caused proportional changes in mercury flux for both absorption and emission (Gillis and Miller, 2000). Aeschlimann and coworkers used a residence time of 15 s during the day and 60 s at night (Aeschlimann et al., 2005), which reflects ambient diurnal variation in friction velocity. Low residence times ensure that chambers are well-mixed, and minimuze reactions between gases in the chamber. However, reducing residence times also reduces the difference in ambient and steady-state trace-gas concentrations in the chamber. Thus, as residence time is decreased, more precise instrumentation is required. We chose to operate our chambers with a 1.5 min residence time, because 1.5 min is sufficiently low to keep environmental conditions close to ambient yet still yield a trace-gas concentration change that is large enough to be detected by inexpensive sensors. This residence time also translates to a flow rate that can be generated with an inexpensive pump. Further reducing the residence time would have required investment in a significantly more expensive pump, as well as more precise sensors, which would undermine the goal of creating an inexpensive flux-measurement system.

Another way that we reduced the cost of the chamber, was by designing our own control system, using inexpensive electronic components. A customized embedded-system platform was used to automate the flux chamber sampling system. The system is based on the low-cost M-Pod air quality monitor (Masson, 2014), with additional instrumentation for pump and actuator control. Firmware running on the common Atmel

AMTD
7, 6877–6915, 2014

(San Jose, CA) Atmega 328 microcontroller controls both the data logging and flux-chamber sampling routine.

Each chamber runs approximately once an hour, and the main vacuum pump is off when the chamber is not sampling. Once per hour, a predefined and automated sampling schedule begins, and the vacuum pump turns on and runs with the lid open for 6.75 min. The pressure change caused by the pump can cause fluctuations in instrument readings, and this bootup time allows the instruments to stabilize before the chamber lid closes. After the 6.75 min initialization, the chamber lid closes, and remains closed for 5 min. It is important to note that the eddy-covariance measurements are fluxes averaged over a 30 min or 1 h time period, and the chamber measurements are a 5 min average, taken every 53 min.

Fluxes were calculated based on the assumption that the chamber was well mixed. A mass balance in the chamber yields the equation,

$$V\frac{\mathrm{d}\mu_j(t)}{\mathrm{d}t} = Q\mu_{j,\mathrm{amb}} - Q\mu_j(t) - F_j A_\mathrm{s}, \tag{5}$$

where $\mu_j(t)$ is the mixing ratio in the chamber of gas, j, with respect to time, Q is the flow rate of air through the chamber, $\mu_{j,\mathrm{amb}}$ is the ambient mixing ratio of gas, j, t is time, A_s is the surface area of the opening at the bottom of the chamber, V is volume of the chamber, and F_j is the flux of gas, j, to the vegetation. Differentiating, $\mu_j(t)$ is found to be

$$\mu_j(t) = \mu_{j,\mathrm{amb}} - \frac{F_j A_\mathrm{s}}{Q}(1 - e^{-\frac{Q}{V}t}). \tag{6}$$

The steady-state solution to this equation, solving for flux, is

$$F = \frac{Q}{A_\mathrm{s}}(\mu_{j,\mathrm{amb}} - \mu_j(\tau_\mathrm{ss})), \tag{7}$$

where τ_ss is the time when the trace-gas concentration in the chamber reaches steady state.

AMTD
7, 6877–6915, 2014

2.5 Gas-phase measurements

Figure 2 shows the flow path of sample air through the chamber. Gas-phase measurements were conducted at the chamber outlet, which consisted of an 11.4 cm diameter PVC pipe. Chamber air was pulled through the outlet via the main vacuum pump. Two 4.76 mm-diameter tubes were attached to the sides of the PVC pipe on one end, and instruments on the other. One tube was connected to a 2B Technologies Model 202 Ozone Monitor, Thermo Scientific Model 42S NO_x analyzer, and LI-COR 7000 H_2O/CO_2 monitor. More information about the instruments is available in Table 2.

The second tube was connected to a small vacuum pump, which moved air through the chamber control box. In addition to the control board, the box housed metal-oxide NO_x and O_3 sensors. Additional data was collected using these commercially available sensors, specifically the Sensortech (Chemlsford, UK) (formerly e2v) MICs-2611 O_3 sensor. All low-cost sensors implemented in the flux-chamber system ranged in cost from USD 10–100, and the O_3 sensors had a detection limit well within typical concentration changes seen in ground-flux measurements. Complex quantification schemes are necessary to quantify the sensor output properly. Such schemes incorporate correction parameters for interference effects. Inexpensive sensor technology has the potential to be incorporated into a flux-chamber system effectively, which would make widespread flux measurements a realizable objective.

2.6 Comparison of eddy-covariance and flux-chamber measurements

Theoretically, dry deposition flux (F) is proportional to the ambient concentration (C) of a trace gas at some reference height (Seinfeld and Pandis, 2006). The proportionality constant between the concentration and flux is called "deposition velocity" (v_d) (Chamberlain and Chadwick, 1953), and

$$F = -v_d C. \quad (8)$$

AMTD
7, 6877–6915, 2014

The deposition process has been described using a resistance analogy (Wesely and Hicks, 2000), in which species transport from the atmosphere to the surface of a material is controlled by three resistances in series.

$$v_d = r_t = r_a + r_b + r_c, \quad (9)$$

where r_t is the total resistance to deposition, r_a is the resistance to aerodynamic transport, r_b is the resistance to diffusion through the quasi-laminar boundary layer, and r_c is the resistance to uptake of a trace gas by the canopy.

This resistance analogy is based on the assumption that the atmosphere is unaltered. It is an accurate analogy for eddy-covariance measurements, but flux chambers alter the wind speed above the canopy, so the resistance analogy must be adjusted. Pape and coworkers proposed an alternate resistance scheme (Pape et al., 2009), which replaces r_a with r_{purge} and r_{mix}, which represent the purging resistance between ambient and chamber air, and mixing in the chamber, respectively. When the chamber is well mixed, r_{mix} is very small, and it can therefore be neglected in this case. r_b is replaced with a modified boundary-layer resistance, r_b^*. r_c should be modified very little by the chamber, provided the chamber does not substantially alter the environmental conditions (temperature, relative humidity) of the natural environment.

Thus, the ratio of chamber flux to ambient flux can be written as

$$\frac{F_{cham}}{F_{amb}} = \frac{r_a + r_b^* + r_c}{r_{purge}} + \rho_d(\mu_{comp} - \mu_{amb}), \quad (10)$$

where ρ_d is the molar density of dry air molecules, and μ_{comp} is the compensation point mixing ratio (Pape et al., 2009).

The results presented in this paper are not corrected using this ratio. While this conversion factor enables chamber flux to be scaled to eddy-covariance flux, it significantly increases the complexity of data processing, and introduces modeling assumptions to an otherwise direct measurement. We present a direct comparison between chamber and eddy-covariance measurements, and will note any bias in chamber measurements.

AMTD
7, 6877–6915, 2014

3 Results and discussion

3.1 Data processing

We collected NO_x, O_3, and CO_2 flux data for 8 days. We used two pairs of identical tall chambers, and one pair of shorter chambers. Each set of data was based on a five-minute sampling period, which occurred once per hour. The flux during each sampling period was assumed to be constant. Each data run was analyzed for noise and pattern, and data sets were either evaluated using Eq. (7) or excluded from results. 9 % of Chamber A data were excluded, 11 % of Chamber B data were excluded, and 0 % of the Chamber C data were excluded.

Figure 3 shows the ozone concentration in the chamber during one sampling period, as an example of ozone data that can be analyzed using the steady-state solution. The area before the decline of the ozone concentration represents the time period when the chamber lid was open. After the lid closed, the concentration began to decline, and eventually reached a steady-state value. This data set met our data-quality requirements, as the data just before the lid closed and at the end of the sample both have low noise, and stay relatively constant for at least one minute. Therefore, the flux was computed using the steady-state solution (Eq. 7).

Figure 4 is an example of a sampling period where the data could not be used to calculate a flux. The ozone concentration increased by an unreasonable amount when the chamber lid opened, which likely indicates malfunction in the 2B ozone monitor.

When the ambient ozone concentration is below 5 ppb, we assume that the ozone flux is zero. Ambient O_3 concentrations of 5 ppb or lower typically occur only at night, when wind speeds are low, which means that the aerodynamic resistance to deposition is high, equating to a low flux. The absolute highest flux rate that could occur, with an ambient concentration of 5 ppb, is 0.09 $\mu g\,m^{-2}\,s^{-1}$ (from Eq. 7), and a flux rate this high is very unlikely with low wind speeds. The median ozone-flux rate measured via eddy covariance, when the ambient ozone concentration was $\leq$ 5 ppb, during the eight-day sampling period, was 0 $\mu g\,m^{-2}\,s^{-1}$, with a standard deviation of 0.05 $\mu g\,m^{-2}\,s^{-1}$.

AMTD
7, 6877–6915, 2014

We did not use the blank chamber data to make any adjustments to the fluxes measured by the dynamic chambers. The median difference between ambient concentration and steady-state ozone concentration was 1.9 ppb for the blank chambers. Since the uncertainty in ozone concentrations, measured by the 2B ozone monitor is ±1.5 ppb, the concentration difference is within a 95 % confidence interval for noise. Thus, correcting chamber fluxes for blank flux would only introduce more error into our measurements.

Also, the median flux measured by the blank chambers, when the open-bottom-chamber flux was nonzero, was $-0.001\,\mu g\,m^{-2}\,s^{-1}$. This value is less than 1 % of the median of the non-zero open-bottom-chamber fluxes, which was $-0.21\,\mu g\,m^{-2}\,s^{-1}$. Therefore, correcting for the blank chamber fluxes would not have a significant impact on measurements. It was encouraging that the blank fluxes were so small, since this indicated that wall losses do not have a significant impact on the flux-chamber measurements. Since wall losses were insignificant, the chamber design could be further simplified by eliminating the blank chambers.

3.2 Photochemistry in the chamber

Photochemical reactions between NO, NO_2, and O_3 can occur in the chamber, and therefore must be considered in Eq. (5) (Meixner et al., 1997; Pape et al., 2009). The primary reactions of concern are

$$NO + O_3 \rightarrow NO_2 + O_2 \quad \text{(R1)}$$

and

$$NO_2 + h\nu \xrightarrow{O_2} NO + O_3,\ \lambda < 420\,\text{nm}. \quad \text{(R2)}$$

Because of the relationships shown in Reactions (R1) and (R2), NO, NO_2 and O_3 must all be measured simultaneously (Pape et al., 2009). Using Reactions (R1) and (R2),

AMTD
7, 6877–6915, 2014

the change in NO and NO_2 mixing ratios is:

$$\frac{d\mu(NO)}{dt} = -k\,\mu(NO)\,\mu(O_3) \quad (11)$$

$$\frac{d\mu(NO)}{dt} = j(NO_2)\,\mu(NO_2), \quad (12)$$

where k is the first-order rate constant of Eq. (R1), and $j(NO_2)$ is the photolysis rate of NO_2 (Pape et al., 2009; Seinfeld and Pandis, 2006). The net source (S_{gp}) of gas-phase NO resulting from Reactions (R1) and (R2) within the chamber, is

$$S_{gp}(NO) = V[j(NO_2)\,\mu_{cham}(NO_2) - k\,\mu_{cham}(NO)\,\mu_{cham}(O_3)]. \quad (13)$$

The rates of formation for NO_2 and O_3 are equal or inversely proportional to the rates of formation for NO, and

$$S_{gp}(NO) = S_{gp}(O_3) = -S_{gp}(NO_2). \quad (14)$$

Combining these reaction sources or sinks with the mass balance from Eqs. (5) and (7) yields

$$V\frac{dC_j(t)}{dt} = Q\mu_{j,amb} - Q\mu_j(t) - F_j A_s + S_{gp}, \quad (15)$$

and

$$F = \frac{Q}{A_s}(\mu_{j,amb} - \mu_j(t)) + \frac{S_{gp}}{A_s}. \quad (16)$$

Pape and coworkers measured $j(NO_2)$ inside their chamber, and found that the average value of $j(NO_2)$ inside the chamber was 48 % of the value outside the chamber (Pape et al., 2009). They fit a curve of $j(NO_2)$ vs. global radiation (G), and we used that

AMTD
7, 6877–6915, 2014

curve in our calculations, since our chambers were similar in shape and material. To quantify the impact of this assumption, we calculated how increasing and decreasing $j(NO_2)$ by 25 % affects ozone flux, and found that this changes ozone flux by < 1 % in all cases. The maximum flux change due to photolysis in all of our results is 1.7 %. Thus, the impact of photolysis on ozone flux was small during our study.

3.3 Ozone results

We measured ozone dry deposition with flux chambers for two days in June, and eight days in September. When compared with eddy-covariance measurements, flux-chamber ozone measurements were able to capture the diurnal flux trends. It is important to remember that eddy-covariance measurements are not without error. For an eddy-covariance system similar to the one used in this study, Finkelstein and Sims (Finkelstein and Sims, 2001) found that mean sampling errors for 30 min average eddy-covariance O_3 fluxes were in the range of 27–33 %.

Figure 5 shows O_3 fluxes measured via eddy covariance, and flux chambers A, B and C, and also calculated using an indirect method, which combined meteorological data and surface-exchange model for the time period between 22 and 28 September. The theory used to calculate the model values is described by Wesely (1989) and Seinfeld and Pandis (2006).

The surface-exchange model results underestimated the mean eddy-covariance flux rate by 26 % between 22 and 27 September. This is a good model-to-measurement match, but it is important to remember that the models do not always predict flux accurately (Wu et al., 2012; Schwede et al., 2011).

Chamber A was moved from its original location in the field to a different position on 24 September. Prior to being moved, the chamber was on a plot of land with a less-prevalent vegetation type, which had a higher LAI than the dominant vegetation (see Fig. 6). After the chamber was moved to a location with more representative vegetation, the data matched the eddy-covariance results much better. Before the chamber was moved (18 and 23 September), the mean ozone-flux rate

AMTD
7, 6877–6915, 2014

measured by eddy-covariance was $-0.16\,\mu g\,m^{-2}\,s^{-1}$, and the mean chamber flux rate was $-0.23\,\mu g\,m^{-2}\,s^{-1}$, which is 48 % higher than the eddy-covariance measurement. After the move (24–27 September), the mean eddy-covariance flux rate was $-0.25\,\mu g\,m^{-2}\,s^{-1}$, and the mean flux measured by the chamber was $-0.26\,\mu g\,m^{-2}\,s^{-1}$, which is 4 % higher than the eddy-covariance measurement. This difference in measurement agreement highlights the importance of selecting a chamber placement that contains vegetation representative of the site.

The LAI in the field, as well as in Chambers A and B, was measured on 11 November. LAI measurements in the open field were made by sampling at regular distances along 100 m transects ($n = 10$ locations) to the southwest and northwest of the eddy-covariance tower (prevailing fetch) with a LI-COR Model LAI-2000 plant canopy analyzer (LI-COR Biosciences, Lincoln, NE). LAI measurements within the chambers were made by inserting the leaf area meter through a port at the bottom of the chamber. Individual measurements consisted of one above-canopy measurement and five below-canopy measurements. Three replicate measurements were taken in each chamber. Measurements within the control chambers showed no difference between above- and below-canopy measurements.

The LAI in the field was between 2.8 and 3.5, the LAI in chamber A was between 2.4 and 2.9, and the LAI in Chamber B was between 2.75 and 3.1. While the chamber-LAI measurements were on the low end of the field measurements, they were inside the range of LAI measurements in the field.

Chamber B operated from 18 to 19 September, and again from 23 to 27 September. The mean ozone flux measured by the flux chamber during this period was $-0.17\,\mu g\,m^{-2}\,s^{-1}$, which is 9 % higher than the mean eddy-covariance ozone flux during the same period ($-0.15\,\mu g\,m^{-2}\,s^{-1}$).

Chamber C, which is the shorter chamber, was operated between 18 and 19 September, and again between 24 and 27 September. The mean chamber flux measured during this period was $-0.115\,\mu g\,m^{-2}\,s^{-1}$, which was 6 % lower than the mean eddy-covariance flux during the same time period ($-0.108\,\mu g\,m^{-2}\,s^{-1}$).

AMTD
7, 6877–6915, 2014

In addition to the September measurements, data were collected for four days in June. The chambers underestimated ozone flux by 50–100 % in June, and we believe that this was because the the LAI was much lower in the chambers than in the field during that time. We did not measure LAI during our June sampling period, but we estimate, by visual inspection, that LAI in the chambers was about 50 % lower in June than in September. The mean grass height in the field did not significantly change between June and November, and measured heights were 42.2 and 43.7 cm, respectively. Further studies that measure ozone deposition with various known LAI values in the chamber could confirm the effects of changing LAI on measured flux.

There was not a systemic bias in the ozone flux data. The excellent agreement between the September flux-chamber and eddy-covariance measurements demonstrates that the flux chamber is capable of measuring ozone flux to grassland ecosystems when the LAI inside the chamber represents the average LAI in the field. Therefore, we conclude that, under the environmental conditions in this study, it is not necessary to use Eq. (10) to scale the dynamic-chamber flux to the eddy-covariance flux.

3.4 Carbon dioxide results

CO_2 data were collected over a 20 h period, beginning at 1.23 p.m. on 18 September, and ending at 9.28 a.m. on 19 September. This short sampling period did not produce enough data to validate chamber performance for CO_2-deposition measurements, but the results look promising. Fluxes were calculated using Eq. (7). Data were examined using the method described in Sect. 3.1. Roughly 1/3 of the data was found to be ineligible for processing.

Figure 7 compares CO_2 fluxes measured using the eddy-covariance and flux-chamber methods. The flux-chamber measurements captured the diurnal CO_2 flux trend. The mean flux rate measured by the flux chamber, for the 12 chamber cycles included, was $-0.03\,mg\,m^{-2}\,s^{-2}$. The eddy-covariance fluxes measured during these 12 h were interpolated to match the flux-chamber times, and the mean flux rate was $-0.08\,mg\,m^{-2}\,s^{-2}$. While this difference seems very large, it is important to remember

AMTD
7, 6877–6915, 2014

that CO_2 fluxes can be both positive and negative. There is not a systematic bias in the data, and the data only represent part of a 20 h period. To make a conclusive flux comparison, it is essential to have at least several 24 h periods of data.

3.5 NO_x results

NO, NO_2, and NO_x fluxes were measured using the dynamic flux chambers for four days, between 18 and 27 September. The mean NO_x concentration at the field site during this time period was 1.79 ppb. While NO_x concentrations are typically low (< 3 ppb), spikes of up to 8.9 ppb were observed during the morning rush hour. Concentrations observed during evening rush hour were not as large as during the morning rush hour, presumably because of the shallow atmospheric boundary layer in the morning.

Flux chamber measurements of NO_x followed the expected pattern for deposition when ambient concentrations were above approximately 1 ppb. Below this concentration, instrument noise exceeded deposition or emissions. Figure 8 shows NO_x concentrations in the chamber in the morning, when ambient concentrations are high. For this time period, the NO_x flux was 20.8 ng m^{-2} s^{-1}, which is a reasonable value for the site. Unfortunately, the eddy-covariance NO_x-flux-measurement system was not functioning during this field campaign. We can conclude that the flux chamber is capable of resolving NO_x fluxes, but further studies, with eddy-covariance flux comparisons, are needed to validate measurement accuracy.

4 Conclusions

Ozone, CO_2, and NO_x deposition onto grassland ecosystems were measured using dynamic flux chambers and eddy covariance. Ozone-deposition measurements from the two methods matched very well (4–10 % difference) when the LAI inside the chambers was representative of the average LAI in the field. This discrepancy is within the uncertainty of eddy covariance, and the flux chambers are considered an accurate

AMTD
7, 6877–6915, 2014

measurement system under these conditions. There was not a bias in the chamber data, when compared with the eddy-covariance data.

When LAI inside the chambers was significantly higher or lower than the rest of the field, chamber measurements over- or under-predicted flux, respectively. A discrepancy between chamber and average LAI values can be caused by both inconsistency in vegetation density and differences in vegetation species. Eddy-covariance systems can only measure net flux to an entire fetch ($> 100\,m^2$), which means that they measure a mean flux to all vegetation in the field, and cannot measure flux to small patches of different vegetation types. Flux chambers are able to measure flux onto different patches of vegetation, which enables the user to understand the relative contribution of different vegetation species to total flux.

We found that the median ozone flux measured by the blank chambers, when the open-bottom-chamber flux was non zero, was $-0.001\,\mu g\,m^{-2}\,s^{-1}$. This value is less than 1 % of the median of the non-zero open-bottom-chamber fluxes, which was $-0.21\,\mu g\,m^{-2}\,s^{-1}$. Therefore, we can conclude that we achieved the design goal of minimizing trace-gas interactions with the walls of the chamber.

CO_2 measurements were conducted for one 20 h period, and the flux chamber captured the diurnal trend in CO_2 flux. The quantity of the data was not sufficient to validate chamber performance, but the results show promise, and additional experiments will be conducted to confirm that the flux chambers can measure CO_2 deposition accurately.

Flux-chamber NO_x measurements were conducted for 4 days, and when ambient NO_x concentrations were above 1 ppb, the data could be used to calculate a NO_x flux. Unfortunately, the eddy-covariance system for measuring NO_x was not available during this field campaign, so comparisons could not be made. However, NO_x fluxes measured by the dynamic chambers did fall in the expected range for the site. Additional experiments will be performed to confirm that the chamber NO_x-flux measurements are accurate.

AMTD
7, 6877–6915, 2014

EPA Disclaimer

This document has been reviewed in accordance with US Environmental Protection Agency policy and approved for publication. The views expressed in this article are those of the author[s] and do not necessarily represent the views or policies of the US Environmental Protection Agency.

Acknowledgements. We are grateful for the opportunity to do this work, which was funded by the Electric Power Research Institute (EPRI). We would like to thank Corey Miller for his help building the flux chambers. We would like to thank Peter Hamlington, Nick Clements, Bill Mitchell, and Andrew Turnipseed for helpful discussions. This project would not have been possible without equipment borrowed from Christine Wiedinmyer and John Ortega, at the National Center for Atmospheric Research, as well as Joanna Gordon and Ashley Collier. Ricardo Piedrahita and Nick Masson's sensor work is the basis for the inexpensive sensor portion of this project.

References

Aeschlimann, U., Nösberger, J., Edwards, P. J., Schneider, M. K., Richter, M., and Blum, H.: Responses of net ecosystem CO_2 exchange in managed grassland to long-term CO_2 enrichment, N fertilization and plant species, Plant Cell Environ., 28, 823–833, 2005. 6887, 6906

Altimir, N., Vesala, T., Keronen, P., Kulmala, M., and Hari, P.: Methodology for direct field measurements of ozone flux to foliage with shoot chambers, Atmos. Environ., 36, 19–29, 2002. 6880, 6906

Aneja, V. P., Robarge, W. P., and Holbrook, B. D.: Measurements of nitric oxide flux from an upper coastal plain, North Carolina agricultural soil, Atmos. Environ., 29, 3037–3042, 1995. 6906

Baldocchi, D. D., Hincks, B. B., and Meyers, T. P.: Measuring biosphere–atmosphere exchanges of biologically related gases with micrometeorological methods, Ecology, 69, 1331–1340, 1988. 6880, 6883

AMTD
7, 6877–6915, 2014

Benedict, K. B., Day, D., Schwandner, F. M., Kreidenweis, S. M., Schichtel, B., Malm, W. C., and Collett Jr, J. L.: Observations of atmospheric reactive nitrogen species in Rocky Mountain National Park and across northern Colorado, Atmos. Environ., 64, 66–76, 2013. 6879

Breuninger, C., Oswald, R., Kesselmeier, J., and Meixner, F. X.: The dynamic chamber method: trace gas exchange fluxes (NO, NO_2, O_3) between plants and the atmosphere in the laboratory and in the field, Atmos. Meas. Tech., 5, 955–989, doi:10.5194/amt-5-955-2012, 2012. 6880, 6906

Breuninger, C., Meixner, F. X., and Kesselmeier, J.: Field investigations of nitrogen dioxide (NO_2) exchange between plants and the atmosphere, Atmos. Chem. Phys., 13, 773–790, doi:10.5194/acp-13-773-2013, 2013. 6880, 6906

Brook, J. R., Zhang, L., Di-Giovanni, F., and Padro, J.: Description and evaluation of a model of deposition velocities for routine estimates of air pollutant dry deposition over North America: Part I: model development, Atmos. Environ., 33, 5037–5051, 1999. 6879

Burkart, S., Manderscheid, R., and Weigel, H.-J.: Design and performance of a portable gas exchange chamber system for CO_2 and H_2O flux measurements in crop canopies, Environ. Exp. Bot., 61, 25–34, 2007. 6906

Butterbach-Bahl, K., Gasche, R., Breuer, L., and Papen, H.: Fluxes of NO and N_2O from temperate forest soils: impact of forest type, N deposition and of liming on the NO and N_2O emissions, Nutr. Cycl. Agroecosys., 48, 79–90, 1997. 6881, 6906

Chamberlain, A. and Chadwick, R. C.: Deposition of airborne radioiodine vapour, Nucleonics, 11, 22–25, 1953. 6889

Dijk, S. M. and Duyzer, J. H.: Nitric oxide emissions from forest soils, J. Geophys. Res.-Atmos., 104, 15955–15961, 1999. 6906

EPA, US: Air Quality Criteria for Ozone and Related Photochemical Oxidants (2006 Final) EPA/600/R-05/004aF, Tech. rep., US Environmental Protection Agency, 2006. 6878, 6879

EPA, US: Clean Air Status and Trends Network 2010 Annual Report, Tech. rep., AMEC Environment & Infrastructure, Inc, prepared for US EPA Under Contract No. EP-W-09-028, 2010. 6879

EPA, US: Policy Assessment for the Review of the Secondary National Ambient Air Quality Standards for Oxides of Nitrogen and Oxides of Sulfur EPA-452-R-11-004a, Tech. rep., United States Environmental Protection Agency, Research Triangle Park, NC, 2011. 6878

Fangmeier, A., Hadwiger-Fangmeier, A., Van der Eerden, L., and Jäger, H.-J.: Effects of atmospheric ammonia on vegetation – a review, Environ. Pollut., 86, 43–82, 1994. 6878, 6879

AMTD
7, 6877–6915, 2014

Fenn, M. E., Poth, M. A., Aber, J. D., Baron, J. S., Bormann, B. T., Johnson, D. W., Lemly, A. D., McNulty, S. G., Ryan, D. F., and Stottlemyer, R.: Nitrogen excess in North American ecosystems: predisposing factors, ecosystem responses, and management strategies, Ecol. Appl., 8, 706–733, 1998. 6878, 6879

Finkelstein, P. and Sims, P.: Sampling error in eddy correlation flux measurements, J. Geophys. Res., 106, 3503–3509, 2001. 6894

Flechard, C. R., Nemitz, E., Smith, R. I., Fowler, D., Vermeulen, A. T., Bleeker, A., Erisman, J. W., Simpson, D., Zhang, L., Tang, Y. S., and Sutton, M. A.: Dry deposition of reactive nitrogen to European ecosystems: a comparison of inferential models across the NitroEurope network, Atmos. Chem. Phys., 11, 2703–2728, doi:10.5194/acp-11-2703-2011, 2011. 6879

Fluxnet: Duke Forest Open Field, available at: http://fluxnet.ornl.gov/site/867 (last access: 14 December 2013), 2013. 6882

Foken, T. and Wichura, B.: Tools for the quality assessment of surface-based flux measurements, Agr. Forest Meteorol., 78, 83–105, 1996. 6885

Garcia, R. L., Norman, J. M., and McDermitt, D. K.: Measurements of canopy gas exchange using an open chamber system, Remote Sensing Reviews, 5, 141–162, 1990. 6906

Geßler, A., Rienks, M., and Rennenberg, H.: NH_3 and NO_2 fluxes between beech trees and the atmosphere–correlation with climatic and physiological parameters, New Phytol., 147, 539–560, 2000. 6880, 6906

Gillis, A. and Miller, D. R.: Some potential errors in the measurement of mercury gas exchange at the soil surface using a dynamic flux chamber, Sci. Total Environ., 260, 181–189, 2000. 6887

Guesten, H., Heinrich, G., Schmidt, R., and Schurath, U.: Tools for the quality assessment of surface-based flux measurements, J. Atmos. Chem., 14, 73–84, 1992. 6884

Gut, A., Neftel, A., Staffelbach, T., Riedo, M., and Lehmann, B.: Nitric oxide flux from soil during the growing season of wheat by continuous measurements of the NO soil–atmosphere concentration gradient: a process study, Plant Soil, 216, 165–180, 1999. 6906

Gut, A., Van Dijk, S., Scheibe, M., Rummel, U., Welling, M., Ammann, C., Meixner, F., Kirkman, G., Andreae, M., and Lehmann, B.: NO emission from an Amazonian rain forest soil: continuous measurements of NO flux and soil concentration, J. Geophys. Res.-Atmos., 107, LBA 24-1–LBA 24-10, doi:10.1029/2001JD0005212002, 2002. 6906

AMTD
7, 6877–6915, 2014

Horst, T.: A simple formula for attenuation of eddy fluxes measured with first-order-response scalar sensors, Bound.-Lay. Meteorol., 82, 219–233, 1997. 6885
Horst, T. and Weil, J.: How far is far enough? The fetch requirements for micrometeorological measurement of surface fluxes, J. Atmos. Ocean. Tech., 11, 1018–1025, 1994. 6880, 6885
Horváth, L., Führer, E., and Lajtha, K.: Nitric oxide and nitrous oxide emission from Hungarian forest soils; linked with atmospheric N-deposition, Atmos. Environ., 40, 7786–7795, 2006. 6906
Kaimal, J. and Finnigan, J.: Atmospheric Boundary-Layer Flows: Their Structure and Measurement, Oxford University Press, 1994. 6885
Kaplan, W., Wofsy, S., Keller, M., and Da Costa, J. M.: Emission of NO and deposition of O_3 in a tropical forest system, J. Geophys. Res.-Atmos., 93, 1389–1395, 1988. 6881, 6906
Kirkman, G., Gut, A., Ammann, C., Gatti, L., Cordova, A., Moura, M., Andreae, M., and Meixner, F.: Surface exchange of nitric oxide, nitrogen dioxide, and ozone at a cattle pasture in Rondonia, Brazil, J. Geophys. Res.-Atmos., 107, LBA 51-1–LBA 51-17, doi:10.1029/2001JD000523, 2002. 6906
Kitzler, B., Zechmeister-Boltenstern, S., Holtermann, C., Skiba, U., and Butterbach-Bahl, K.: Nitrogen oxides emission from two beech forests subjected to different nitrogen loads, Biogeosciences, 3, 293–310, doi:10.5194/bg-3-293-2006, 2006. 6881, 6906
Laville, P., Lehuger, S., Loubet, B., Chaumartin, F., and Cellier, P.: Effect of management, climate and soil conditions on N_2O and NO emissions from an arable crop rotation using high temporal resolution measurements, Agr. Forest Meteorol., 151, 228–240, 2011. 6906
Li, Y., Aneja, V. P., Arya, S., Rickman, J., Brittig, J., Roelle, P., and Kim, D.: Nitric oxide emission from intensively managed agricultural soil in North Carolina, J. Geophys. Res.-Atmos., 104, 26115–26123, 1999. 6906
Machon, A., Horváth, L., Weidinger, T., Grosz, B., Pintér, K., Tuba, Z., and Führer, E.: Estimation of net nitrogen flux between the atmosphere and a semi-natural grassland ecosystem in Hungary, Eur. J. Soil Sci., 61, 631–639, 2010. 6906
Maljanen, M., Martikkala, M., Koponen, H. T., Virkajärvi, P., and Martikainen, P. J.: Fluxes of nitrous oxide and nitric oxide from experimental excreta patches in boreal agricultural soil, Soil Biol. Biochem., 39, 914–920, 2007. 6906
Masson, N.: UPOD: An open-source platform for air quality monitoring, available at: http://mobilesensingtechnology.com/ (last access: 10 January 2014), 2014. 6887

AMTD
7, 6877–6915, 2014

Meixner, F., Fickinger, T., Marufu, L., Serca, D., Nathaus, F., Makina, E., Mukurumbira, L., and Andreae, M.: Preliminary results on nitric oxide emission from a southern African savanna ecosystem, Nutr. Cycl. Agroecosys., 48, 123–138, 1997. 6881, 6892, 6906

Muller, J. B. A., Percival, C. J., Gallagher, M. W., Fowler, D., Coyle, M., and Nemitz, E.: Sources of uncertainty in eddy covariance ozone flux measurements made by dry chemiluminescence fast response analysers, Atmos. Meas. Tech., 3, 163–176, doi:10.5194/amt-3-163-2010, 2010. 6885

Musselman, R. C., Lefohn, A. S., Massman, W. J., and Heath, R. L.: A critical review and analysis of the use of exposure and flux-based ozone indices for predicting vegetation effects, Atmos. Environ., 40, 1869–1888, 2006. 6879

Norman, J., Kucharik, C., Gower, S., Baldocchi, D., Crill, P., Rayment, M., Savage, K., and Striegl, R.: A comparison of six methods for measuring soil-surface carbon dioxide fluxes, J. Geophys. Res.-Atmos., 102, 28771–28777, 1997. 6881, 6906

Pape, L., Ammann, C., Nyfeler-Brunner, A., Spirig, C., Hens, K., and Meixner, F. X.: An automated dynamic chamber system for surface exchange measurement of non-reactive and reactive trace gases of grassland ecosystems, Biogeosciences, 6, 405–429, doi:10.5194/bg-6-405-2009, 2009. 6880, 6881, 6887, 6890, 6892, 6893, 6906

Parrish, D. D., Williams, E. J., Fahey, D. W., Liu, S. C., and Fehsenfeld, F. C.: Measurement of nitrogen oxide fluxes from soils: Intercomparison of enclosure and gradient measurement techniques, J. Geophys. Res.-Atmos., 92, 2165–2171, 1987. 6881, 6906

Pilegaard, K.: Air–soil exchange of NO, NO_2 and O_3 in forests, Water Air Soil Pollut.: Focus, 1, 79–88, 2001. 6906

Pilegaard, K., Hummelshøj, P., and Jensen, N.: Nitric oxide emission from a Norway spruce forest floor, J. Geophys. Res.-Atmos., 104, 3433–3445, 1999. 6906

Remde, A., Ludwig, J., Meixner, F. X., and Conrad, R.: A study to explain the emission of nitric oxide from a marsh soil, J. Atmos. Chem., 17, 249–275, 1993. 6881, 6906

Roelle, P., Aneja, V. P., O'connor, J., Robarge, W., Kim, D.-S., and Levine, J. S.: Measurement of nitrogen oxide emissions from an agricultural soil with a dynamic chamber system, J. Geophys. Res.-Atmos., 104, 1609–1619, 1999. 6906

Roelle, P. A., Aneja, V. P., Gay, B., Geron, C., and Pierce, T.: Biogenic nitric oxide emissions from cropland soils, Atmos. Environ., 35, 115–124, 2001. 6906

SAS Institute: Version 9.3 System Help, 2003. 6884

AMTD
7, 6877–6915, 2014

Schwede, D. B. and Lear, G. G.: A novel hybrid approach for estimating total deposition in the United States, Atmos. Environ., 92, 207–220, 2014. 6879

Schwede, D. B., Zhang, L., Vet, R., and Lear, G.: An intercomparison of the deposition models used in the CASTNET and CAPMoN networks, Atmos. Environ., 45, 1337–1346, 2011. 6879, 6894

Seinfeld, J. H. and Pandis, S. N.: Atmospheric Chemistry and Physics, 2nd edn., Wiley, 2006. 6879, 6880, 6889, 6893, 6894

Skiba, U., Smith, K. A., and Fowler, D.: Nitrification and denitrification as sources of nitric oxide and nitrous oxide in a sandy loam soil, Soil Biol. Biochem., 25, 1527–1536, 1993. 6906

Slemr, F. and Seiler, W.: Field measurements of NO and NO_2 emissions from fertilized and unfertilized soils, J. Atmos. Chem., 2, 1–24, 1984. 6906

Sparks, J. P., Monson, R. K., Sparks, K. L., and Lerdau, M.: Leaf uptake of nitrogen dioxide (NO_2) in a tropical wet forest: implications for tropospheric chemistry, Oecologia, 127, 214–221, 2001. 6880, 6906

Stella, P., Loubet, B., Laville, P., Lamaud, E., Cazaunau, M., Laufs, S., Bernard, F., Grosselin, B., Mascher, N., Kurtenbach, R., Mellouki, A., Kleffmann, J., and Cellier, P.: Comparison of methods for the determination of NO-O_3-NO_2 fluxes and chemical interactions over a bare soil, Atmos. Meas. Tech., 5, 1241–1257, doi:10.5194/amt-5-1241-2012, 2012. 6881, 6906

Turnipseed, A., Burns, S., Moore, D., Hu, J., Guenther, A., and Monson, R.: Controls over ozone deposition to a high elevation subalpine forest, Agr. Forest Meteorol., 149, 1447–1459, 2009. 6880

Unsworth, M., Heagle, A., and Heck, W.: Gas exchange in open-top field chambers – I. Measurement and analysis of atmospheric resistances to gas exchange, Atmos. Environ., 18, 373–380, 1984. 6906

Webb, E. K., Pearman, G. I., and Leuning, R.: Correction of flux measurements for density effects due to heat and water vapour transfer, Q. J. Roy. Meteor. Soc., 106, 85–100, 1980. 6885

Wesely, M.: Parameterization of surface resistances to gaseous dry deposition in regional-scale numerical models, Atmos. Environ., 23, 1293–1304, 1989. 6894

Wesely, M. and Hicks, B. B.: A review of the current status of knowledge on dry deposition, Atmos. Environ., 34, 2261–2282, 2000. 6879, 6890

AMTD
7, 6877–6915, 2014

Williams, E. and Davidson, E.: An intercomparison of two chamber methods for the determination of emission of nitric oxide from soil, Atmos. Environ. A-Gen., 27, 2107–2113, 1993. 6906

Williams, M. and Tonnessen, K.: Critical loads for inorganic nitrogen deposition in the Colorado Front Range, USA, Ecol. Appl., 10, 1648–1665, 2000. 6878, 6879

Wu, W., Zhang, G., and Kai, P.: Ammonia and methane emissions from two naturally ventilated dairy cattle buildings and the influence of climatic factors on ammonia emissions, Atmos. Environ., 61, 232–243, 2012. 6894

Wu, Z., Wang, X., Chen, F., Turnipseed, A. A., Guenther, A. B., Niyogi, D., Charusombat, U., Xia, B., William Munger, J., and Alapaty, K.: Evaluating the calculated dry deposition velocities of reactive nitrogen oxides and ozone from two community models over a temperate deciduous forest, Atmos. Environ., 45, 2663–2674, 2011. 6879

Yamulki, S., Goulding, K., Webster, C., and Harrison, R. M.: Studies on NO and N_2O fluxes from a wheat field, Atmos. Environ., 29, 1627–1635, 1995. 6906

Zahn, A., Weppner, J., Widmann, H., Schlote-Holubek, K., Burger, B., Kühner, T., and Franke, H.: A fast and precise chemiluminescence ozone detector for eddy flux and airborne application, Atmos. Meas. Tech., 5, 363–375, doi:10.5194/amt-5-363-2012, 2012. 6884

Zhang, L., Moran, M., and Brook, J.: A comparison of models to estimate in-canopy photosynthetically active radiation and their influence on canopy stomatal resistance, Atmos. Environ., 35, 4463–4470, 2001. 6879

Zhang, L., Brook, J. R., and Vet, R.: A revised parameterization for gaseous dry deposition in air-quality models, Atmos. Chem. Phys., 3, 2067–2082, doi:10.5194/acp-3-2067-2003, 2003. 6879

AMTD
7, 6877–6915, 2014

Table 1. Summary of selected chamber measurements of NO_2, NO, O_3, and CO_2.

Reference	Gases Measured	Surface	Chamber Type	Validation Method
Aeschlimann et al. (2005)	CO_2	grassland	dynamic	none
Altimir et al. (2002)	CO_2, O_3	Scots Pine Shoots	dynamic, shoot chamber	compared w/typical O_3 flux values
Aneja et al. (1995)	NO_2, NO	Agricultural Soil	dynamic	none
Breuninger et al. (2012)	NO_2, NO, CO_2, O_3	Norway Spruce	dynamic, branch chamber	none
Breuninger et al. (2013)	NO_2, NO, CO_2, O_3	Norway Spruce	dynamic, branch chamber	none
Burkart et al. (2007)	CO_2	barley, sugar beet, wheat	dynamic	destructive harvest
Butterbach-Bahl et al. (1997)	NO_2, NO, O_3	forest soil	dynamic, automated lid	none
Garcia et al. (1990)	CO_2	soybeans	dynamic	none
Geßler et al. (2000)	NO_2, CO_2, NH_3	beech saplings and twigs	dynamic	none
Gut et al. (1999)	NO	wheat	dynamic	model comparison
Gut et al. (2002)	NO_2, NO, CO_2, O_3	soil	dynamic	model comparison (using ambient concentration)
Horváth et al. (2006)	NO, O_3	spruce and oak soil	dynamic	none
Kaplan et al. (1988)	NO	forest soil	dynamic	compared well with nighttime vertical profile
Kirkman et al. (2002)	NO_2, NO, O_3	pasture	dynamic	none
Kitzler et al. (2006)	NO_2, CO_2	forest soil	dynamic, automated lid	none
Laville et al. (2011)	NO, CO_2	agricultural soil	dynamic, automated lid	none
Li et al. (1999)	NO	agricultural soil	dynamic	chamber values larger than eddy-covariance, but varied similarly with time
Machon et al. (2010)	NO	grassland	dynamic	compared with model
Maljanen et al. (2007)	NO	dung and urine patches on soil	dynamic	none
Meixner et al. (1997)	NO, NO_2, O_3	grassland and crops	dynamic, automated lid	none
Norman et al. (1997)	CO_2	forest soil	dynamic and static	compared 5 types of chambers and 2 eddy-covariance data points
Pape et al. (2009)	NO_2, NO, CO_2, O_3	grassland	dynamic, automatic lid	very good agreement w/eddy covariance for CO_2 (did not compare NO, NO_2, and O_3)
Parrish et al. (1987)	NO	grassland	dynamic	nighttime comparison with gradient method
Pilegaard et al. (1999)	NO, CO_2	forest soil	dynamic	none
Pilegaard (2001)	NO, NO_2, O_3	forest soil	dynamic, automated lid	none
Remde et al. (1993)	NO, NO_2, O_3	marsh soil	dynamic	none
Roelle et al. (1999)	NO, NO_2	corn soil	dynamic	none
Roelle et al. (2001)	NO	agricultural soils	dynamic	none
Skiba et al. (1993)	NO	ryegrass	dynamic	none
Slemr and Seiler (1984)	NO, NO_2	grassland soil	dynamic	none
Sparks et al. (2001)	NO_2	25 leaf species	dynamic leaf chamber	none
Stella et al. (2012)	NO	agricultural soil	dynamic, automated lid	agreed with gradient method for low fluxes, but underestimated high fluxes
Unsworth et al. (1984)	O_3	soybeans	dynamic, open top	canopy resistances comparable to other field studies
Dijk and Duyzer (1999)	NO	forest soil	dynamic	none
Williams and Davidson (1993)	NO	grassland	dynamic	comparison of 2 chamber types
Yamulki et al. (1995)	NO	agricultural soil	dynamic	none

AMTD
7, 6877–6915, 2014

Table 2. Trace gas detectors, with manufacturers' specifications.

Gas	Detection Method	Manufacturer and Model	Detection Limit	Precision
O_3	UV Light Absorption	2b Technologies (Boulder, CO) 202	1.5 ppb	± 1.5 ppb
NO_x	chemiluminescence	Thermo Scientific (Waltham, MA) 42S	0.4 ppb	± 0.4 ppb
CO_2	non-dispersive infrared gas analyzer	LI-COR (Lincoln, NE) 7000	0 ppm	0.01 ppm
H_2O	non-dispersive infrared gas analyzer	LI-COR (Lincoln, NE) 7000	0 ppm	0.01 ppm

AMTD
7, 6877–6915, 2014

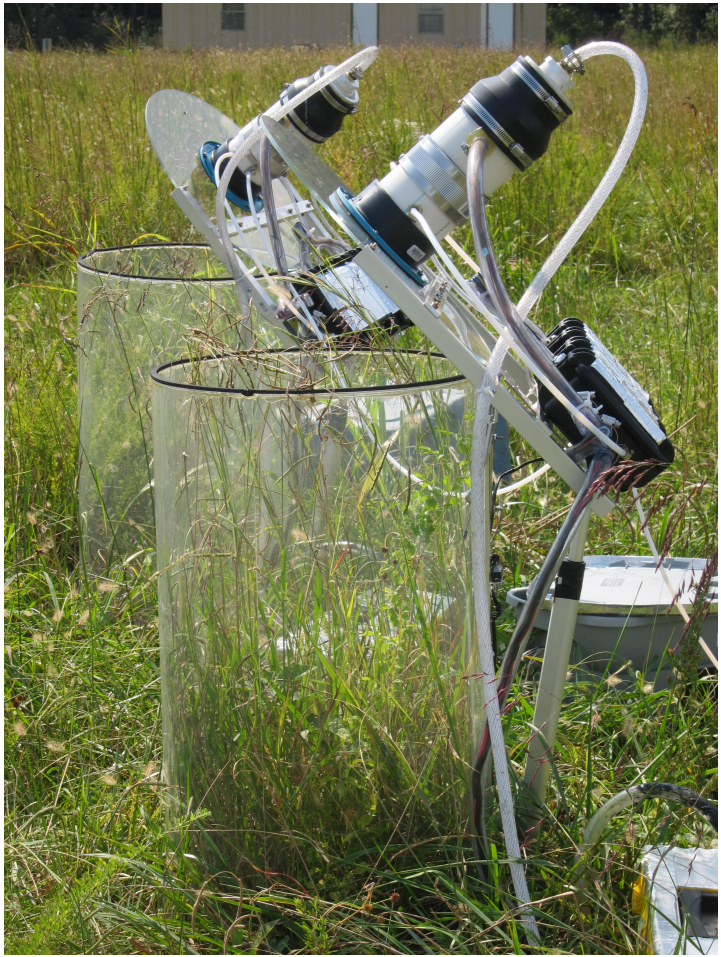

Figure 1. The photo above shows a pair of flux chambers at the field site in the Duke Forest.

AMTD
7, 6877–6915, 2014

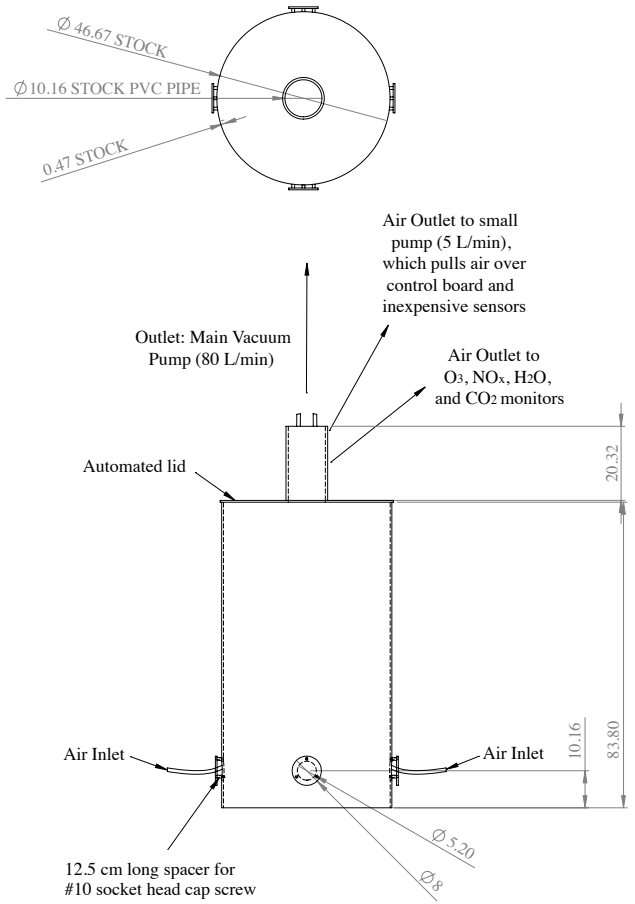

Figure 2. The plot above shows the dimensions of the chamber, and the locations of the air inlets and outlet.

AMTD
7, 6877–6915, 2014

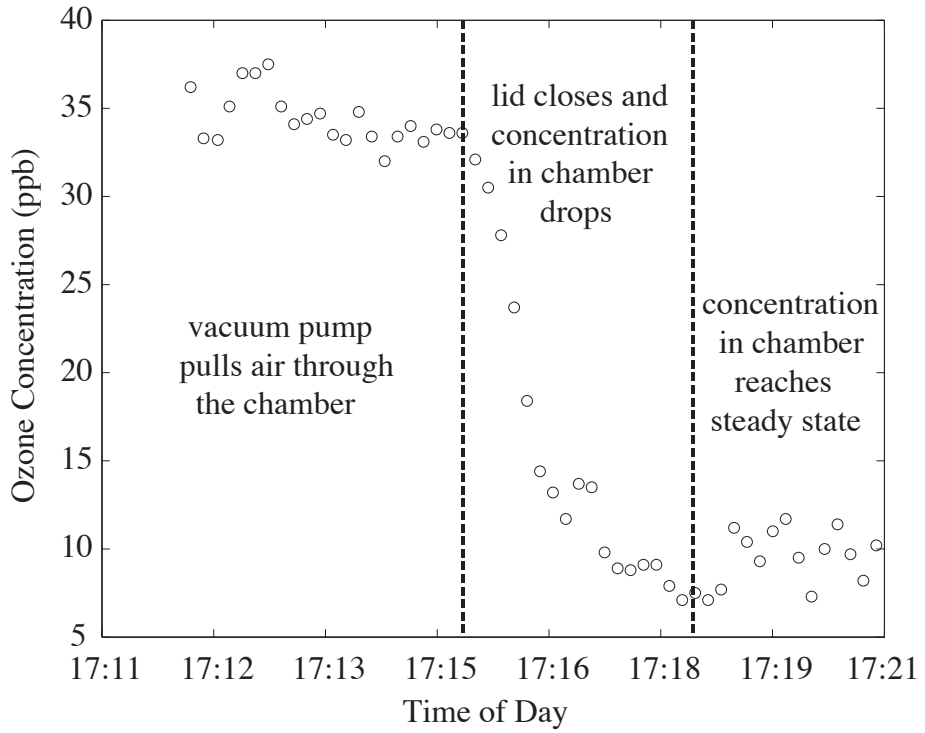

Figure 3. The plot above is an example of ozone data that can be analyzed using the steady-state mass-balance equation. The data before the lid is closed and at the end of the sample both have low noise, and stay relatively constant for at least one minute.

AMTD
7, 6877–6915, 2014

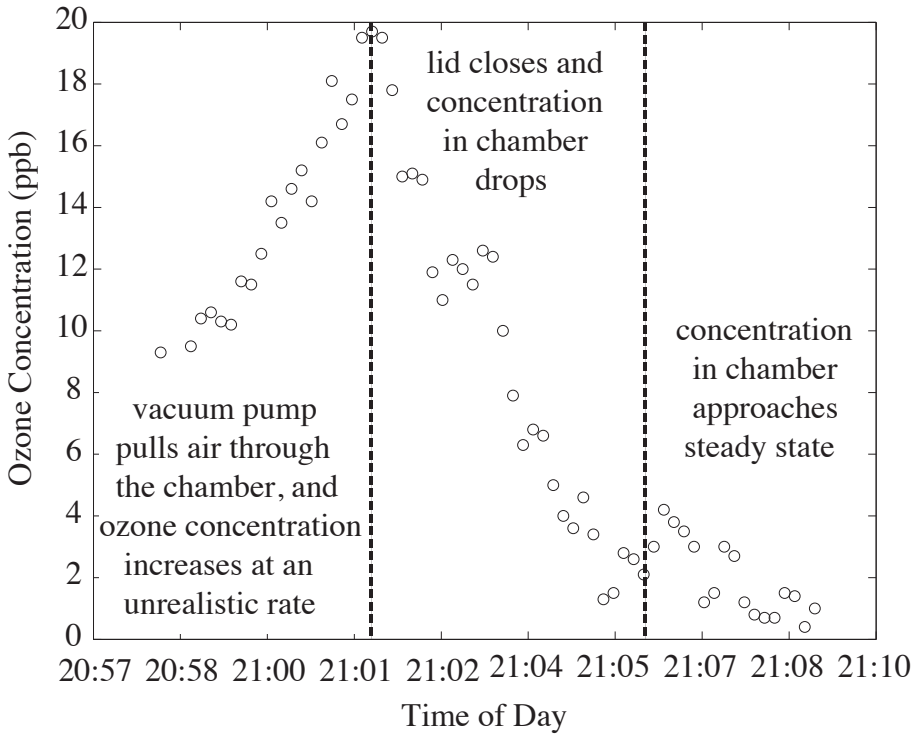

Figure 4. The plot above is an example of a run where we the data could not be used to calculate a flux. The ozone concentration increases by an unreasonable amount when the chamber lid opens, which likely indicated malfunction in the 2B ozone monitor.

AMTD
7, 6877–6915, 2014

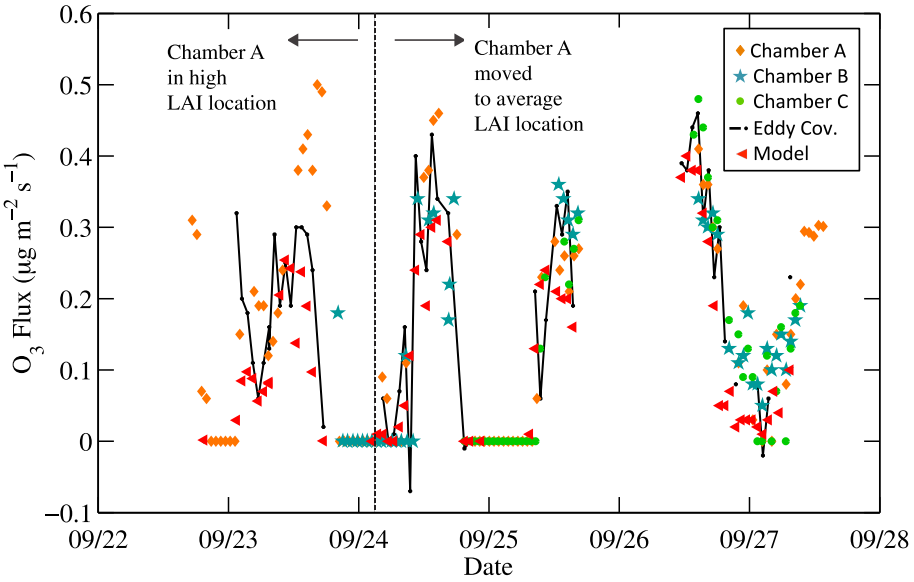

Figure 5. The plot above compares O_3 fluxes measured using eddy covariance (solid black line and black dots), surface-exchange modeling (red triangles), and flux chambers A (orange diamonds), B (blue stars), and C (green dots). The tick marks represent midnight on the date listed.

AMTD
7, 6877–6915, 2014

Figure 6. Chamber A (left). Chamber B (right) – The vegetation in Chamber A, prior to being moved on 24 September, was not representative of the typical vegetation type or LAI at the site. As a result, flux measurements prior to the move were large when compared with measurements from other chambers and eddy covariance. The vegetation in Chamber B was representative of the vegetation in the field.

AMTD
7, 6877–6915, 2014

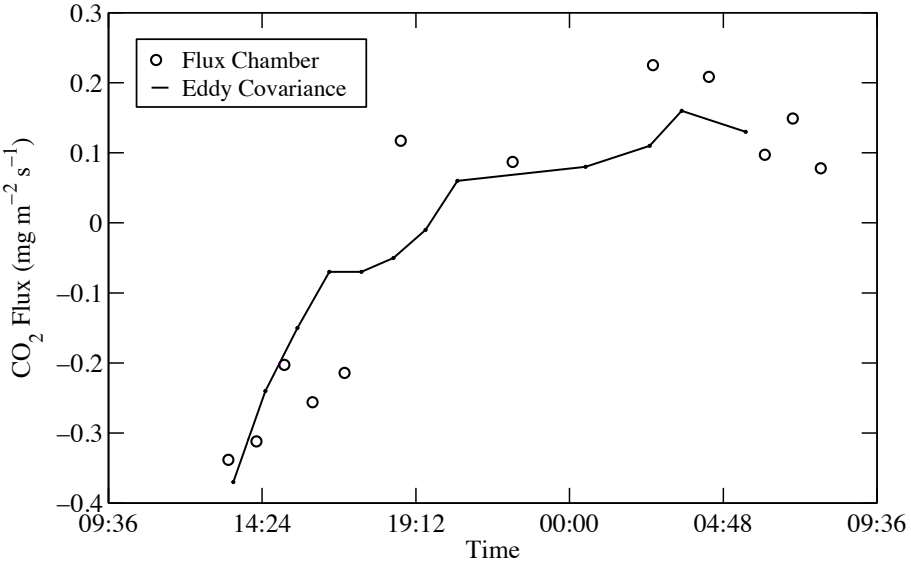

Figure 7. The plot above compares CO_2 fluxes measured using the eddy covariance (line) and flux chamber (stars) methods.

AMTD
7, 6877–6915, 2014

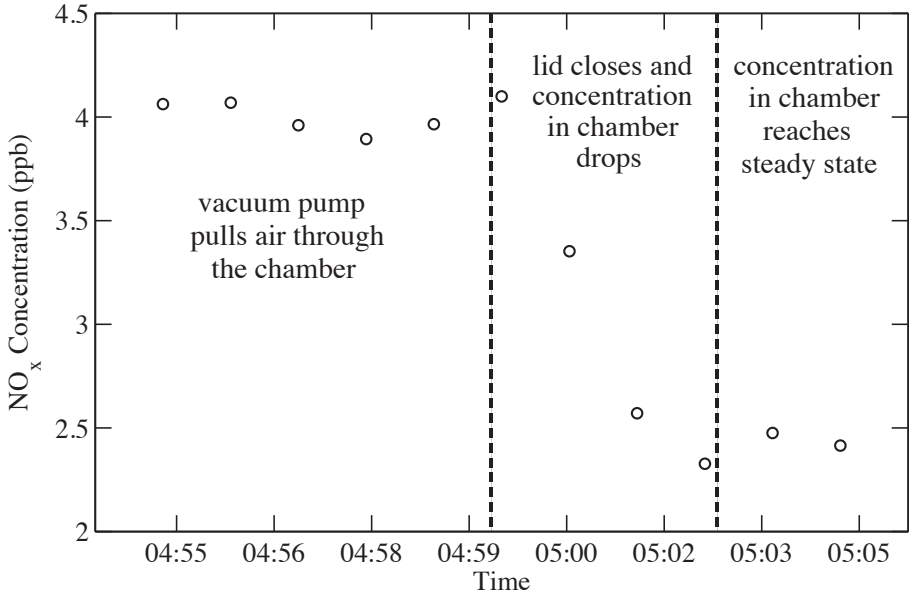

Figure 8. The plot above shows NO_x fluxes in the flux chamber during a morning sampling routine.

AMTD
7, 6877–6915, 2014